Thermal neutron capture cross section for ^{56}Fe(n,γ)

R. B. Firestone,[1,2] T. Belgya,[3] M. Krtička,[4] F. Bečvář,[4] L. Szentmiklósi,[3] and I. Tomandl[5]
[1]*University of California, Department of Nuclear Engineering, Berkeley, California 94720, USA*
[2]*Lawrence Berkeley National Laboratory, Berkeley, California 94720, USA*
[3]*Centre for Energy Research, Hungarian Academy of Sciences, H-1525 Budapest, Hungary*
[4]*Charles University in Prague, Faculty of Mathematics and Physics, V. Holešovičkách 2, CZ-180 00 Prague 8, Czech Republic*
[5]*Nuclear Physics Institute, Czech Academy of Sciences, CZ-250 68 Řež, Czech Republic*
(Received 24 October 2016; published 30 January 2017)

The ^{56}Fe(n,γ) thermal neutron capture cross section and the ^{57}Fe level scheme populated by this reaction have been investigated in this work. Singles γ-ray spectra were measured with an isotopically enriched ^{56}Fe target using the guided cold neutron beam at the Budapest Reactor, and $\gamma\gamma$-coincidence data were measured with a natural Fe target at the LWR-15 research reactor in Řež, Czech Republic. A detailed level scheme consisting of 448 γ rays populating/depopulating 97 levels and the capture state in ^{57}Fe has been constructed, and ≈99% of the total transition intensity has been placed. The transition probability of the 352-keV γ ray was determined to be $P_\gamma(352) = 11.90 \pm 0.07$ per 100 neutron captures. The ^{57}Fe level scheme is substantially revised from earlier work and ≈33 previously assigned levels could not be confirmed while a comparable number of new levels were added. The ^{57}Fe γ-ray cross sections were internally calibrated with respect to ^{1}H and ^{32}S γ-ray cross section standards using iron(III) acetylacetonate ($C_{15}H_{21}FeO_6$) and iron pyrite (FeS_2) targets. The thermal neutron cross section for production of the 352-keV γ-ray cross section was determined to be $\sigma_\gamma(352) = 0.2849 \pm 0.015$ b. The total ^{56}Fe(n,γ) thermal radiative neutron cross section is derived from the 352-keV γ-ray cross section and transition probability as $\sigma_0 = 2.394 \pm 0.019$ b. A least-squares fit of the γ rays to the level scheme gives the ^{57}Fe neutron separation energy $S_n = 7646.183 \pm 0.018$ keV.

DOI: 10.1103/PhysRevC.95.014328

I. INTRODUCTION

Precise thermal neutron capture γ-ray spectra were measured for all elements with $Z = 1$–83, 90, and 92, except for He and Pm, using neutron beams at the Budapest Reactor [1,2]. The γ-ray energies and cross sections were determined and combined, together with additional information from the literature, to generate the Evaluated Gamma-ray Activation File (EGAF) [3] and they were also published in the *Handbook of Prompt Gamma Activation Analysis with Neutron Beams* [4]. These data can be used to determine total radiative thermal neutron capture cross sections, σ_0. When the level scheme is complete, σ_0 equals both the sum of transition cross sections, γ-ray plus conversion electron, feeding the ground state (GS), $\Sigma\sigma_{\gamma+e}$(GS), and the sum of transition cross sections deexciting the capture state (CS), $\Sigma\sigma_{\gamma+e}$(CS). Thermal neutron capture decay schemes are typically completely determined for low-Z elements where all of the transitions are observed.

Iron is an important structural and shielding material in nuclear reactors and other nuclear installations that has an important impact on thermal neutron flux distribution in a reactor pressure vessel [5]. Despite its importance, the ^{56}Fe(n,γ) total radiative thermal neutron cross section, σ_0, is only known to an accuracy of ≈5% based on only two early measurements from over 40 years ago. In this work the ^{56}Fe(n,γ) reaction has been studied with a thermal equivalent neutron beam impinging on an enriched ^{56}Fe target. The corresponding ^{57}Fe γ-ray decay scheme has been nearly completely determined with only minor corrections necessary to account for the weak, missing, or unplaced γ-ray intensity. The new γ-ray data have been internally calibrated with thermal cross section γ-ray standards to determine a new value of the total radiative thermal neutron cross section accurate to ≈0.8%.

The ^{56}Fe(n,γ) reaction was previously studied by Vennink *et al.* [6], who placed 191 γ rays that populated/depopulated 62 levels in ^{57}Fe. Levels and γ rays were assigned by Vennink *et al.* on the basis of γ-ray energy sums but without the aid of $\gamma\gamma$ coincidence data. That procedure can be unreliable due to a high probability of chance energy sums matching known level energies resulting from the complexity of the (n,γ) spectrum. In this work we have also exploited $\gamma\gamma$ coincidence spectra, originally measured for studying two-step γ cascades [7] using a natural Fe target, to confirm the placement of more than 70% of the transitions observed in γ-ray singles measurements, add new transitions, and divide the intensities of γ rays that could be multiply placed in the decay scheme.

II. EXPERIMENT

The singles ^{56}Fe(n,γ) neutron capture γ-ray spectrum was measured in the guided cold neutron beam at the 10-MW Budapest Reactor [1]. Neutrons entered the evacuated target holder and continued to the beam stop at the rear wall of the guide hall. The target station, where both primary and secondary γ rays can be measured in low background conditions, is located 30 m from the reactor. The thermal-equivalent neutron flux at the target was 1.2×10^8 cm^{-2} s^{-1} during this experiment.

Prompt γ rays from the target were measured with an n-type high-purity, 27% efficient, germanium (HPGe) detector with closed-end coaxial geometry located 23.5 cm from the target. The detector is Compton-suppressed by a bismuth germanate

TABLE I. ^{56}Fe(n,γ) thermal neutron capture γ ray energies and relative intensities measured in this work for γ energies from 14 to 352 keV, with detailed transition characteristics.

E_γ (keV)	I_γ [a]	Multipolarity [12]	Mixing ratio δ [12]	ICC [13]	Placement (initial → final)
14.4130(3) [b,c]	55.0(4)	$M1+E2$	0.00223(1)	8.54(2)	14 → 0
92(1) [d]	0.08(3)	[$M1$]		0.044(2)	7646 → 7554
105.5(3)	0.051(17)				unplaced
119.86(11) [e]	0.172(25)	$M1$		0.0218(3)	3547 → 3428
122.026(14) [c]	35.4(6)	$M1+E2$	0.120(1)	0.0238(4)	136 → 14
134.00(24)	0.046(12)				unplaced
136.441(16) [c]	4.51(8)	$E2$		0.149(2)	136 → 0
186.7(4) [e]	0.020(10)	[$M1$]		0.007(1)	5495 → 5308
200.60(21)	0.068(13)				unplaced
204.52(24)	0.064(13)				unplaced
230.298(13) [c]	9.70(14)	[$M1$]		0.0042(1)	367 → 136
318.96(6) [e]	0.131(11)	[$M1$]		0.00190(3)	3240 → 2921
325(1) [d]	0.5(2)	[$M1$]		0.00181(3)	7646 → 7321
333(1) [c]	0.22(8)	[$M1$]		0.00171(3)	7646 → 7313
339.618(14) [f]	1.61(3)	[$M1$]		0.00164(2)	706 → 367
350(1) [g]	0.29(10)	[$M1$]		0.00152(2)	1357 → 1007
352.347(13) [c]	100.0(14)	$M1+E2$	0.025(9)	0.0029(15)	367 → 14

[a]Relative intensity. For multiply placed transitions the singles γ-ray intensity has been divided on the basis of intensity balance and coincidence data. Multiply by 0.1190(7) for transition probability per 100 neutron captures, $P_\gamma(\%)$.
[b]Not observed. Intensity calculated from intensity balance feeding the 14.4-keV level and corrected for unobserved continuum feeding (see text).
[c]Transition confirmed by coincidence data.
[d]Expected primary γ-ray transition, see text.
[e]Transition placed by energy sums.
[f]Transition adopted from ENSDF [12].
[g]Transition proposed from intensity balance but likely obscured by strong 352-keV γ-ray.

(BGO) scintillator guard detector annulus surrounded by 10-cm-thick lead shielding. Relative detection efficiency was calibrated from 50 keV to 10 MeV with radioactive sources and (n,γ) reaction γ rays to a precision of better than 1% from 500 keV to 6 MeV and better than 2% at 100–500 keV and >6 MeV [8]. The γ-ray spectra were analyzed using the HYPERMET PC program [8,9].

An FeO target enriched to 99.94% in ^{56}Fe, suspended in a Teflon bag to minimize background from the target holder, was irradiated to obtain a high statistics, impurity free ^{57}Fe spectrum. No target impurity γ rays were observed in the prompt γ-ray spectrum, verifying that nearly all of the observed γ rays could be assigned to ^{57}Fe. Elemental radiative thermal neutron γ-ray cross sections were normalized, with respect to hydrogen and sulfur standard γ rays, using stoichiometric high purity iron(III) acetylacetonate ($C_{15}H_{21}FeO_6$) and iron pyrite (FeS_2) targets where the isotopic cross sections were determined from the ^{56}Fe natural abundance [10].

Coincidence data were measured at the LWR-15 research reactor in Řež with two HPGe detectors, with efficiencies of 20% and 25% respectively, placed above and below the horizontally situated target with their axes parallel to each other. Sum coincidence gates were set on γ rays deexciting the capture state and populating levels at 0, 14, 136, 367, 706, 1265, 1627, 1725, 2118, and 2207 keV in ^{57}Fe via two-step cascades. The two-step coincidence method is described in detail by Honzátko *et al.* [11].

III. ^{57}Fe DECAY SCHEME

A total of 472 γ-ray transitions, including numerous unresolved multiplets, were assigned to the ^{56}Fe(n,γ) reaction and 448 γ-rays were placed in the ^{57}Fe level scheme; they are summarized in Tables I and II. The low energy 14.4-keV transition connecting the first excited and ground states was not observed in this work, and its intensity has been inferred from the total intensity feeding the 14.4-keV level. Most transition placements were confirmed by the sum coincidence data. Other γ rays were previously placed on the basis of previous work in the Evaluated Nuclear Structure Data File (ENSDF) evaluation [12]. Some γ rays were placed on the basis of energy sums and intensity balance considerations. The intensities of the unresolved multiplets were divided on the basis of coincidence data and the decay scheme intensity balance. The 92-, 325-, and 333-keV primary γ rays were too weak to be observed but are assumed to exist because they feed levels that are too high in excitation energy to be significantly populated by other weakly fed, higher-lying states. The γ-rays at 7313 and 7554 keV are arbitrarily assumed to populate the GS. They are too weak to be observed in the coincidence data. The level at 7321 keV was placed on the basis that the 7306.5-keV transition is very weakly observed in sum coincidence with the 14-keV level, and a 1346.58-keV γ ray can be placed deexciting this level to the 5975-keV level on the basis of energy sums. Expected $E1$ primary γ rays populating the 2554.12-, 2574.07-, and

TABLE II. $^{56}Fe(n,\gamma)$ thermal neutron capture γ ray energies and relative intensities measured in this work for γ energies of 366 keV and higher.

E_γ (keV)	I_γ[a]	Placement (initial → final)
366.752(13)[b]	18.03(25)	367 → 0
460.42(7)[b]	0.685(23)	1725 → 1265
487.9(4)	0.013(9)	unplaced
490.92(11)[b]	0.061(14)	2118 → 1627
525.91(10)[b]	0.063(12)	7646 → 7120
566.4(3)[c]	0.024(8)	4548 → 3982
569.966(15)[d]	4.78(7)	706 → 136
628.59(9)[b]	0.112(11)	2836 → 2207
635.33(8)[c]	0.104(11)	6676 → 6040
640.50(18)[d]	0.051(11)	1007 → 367
650.70(3)[d]	1.71(3)	1357 → 706
665.66(7)[c]	0.184(18)	3240 → 2574
689.8(5)[c]	0.16(4)	5238 → 4548
692.005(14)[b]	50.9(7)	706 → 14
706.42(4)[b]	2.14(4)	706 → 0
717.9(4)[b]	0.070(17)	2836 → 2118
731.07(10)[c]	0.179(16)	6160 → 5429
734.90(8)[d]	0.617(23)	3240 → 2505
746.49(12)	0.082(21)	unplaced
761.10(4)[c]	0.273(19)	2118 → 1357
779.68(14)[b]	0.063(9)	2505 → 1725
809(1)[b]	0.44(15)	7646 → 6837
821.04(6)[c]	0.171(15)	3792 → 2971
834.9(5)[c]	0.014(13)	5084 → 4249
849.7(4)[c]	0.050(14)	3547 → 2697
853.0(6)[c]	0.024(13)	3428 → 2574
855.89(17)[b]	0.095(15)	7646 → 6790
867.82(22)[b]	0.086(19)	7646 → 6778
870.68(8)[d]	1.21(4)	1007 → 136
873.2(4)[c]	0.047(15)	3428 → 2554
877.0(3)[c]	0.083(15)	4249 → 3371
894.1(4)	0.060(15)	unplaced
898.251(15)[b]	19.4(3)	1265 → 367
900.68(6)[b]	0.324(20)	7646 → 6746
911.67(20)[c]	0.055(13)	4209 → 3298
920.843(15)[b]	7.71(11)	1627 → 706
922(1)[b]	0.12(6)	7646 → 6724
950.2(3)[c]	0.035(13)	4249 → 3298
955.79(11)[c]	0.115(17)	3792 → 2836
970.48(12)[b]	0.144(19)	7646 → 6676
987.52(20)	0.063(16)	unplaced
990.42(11)[d]	0.574(22)	1357 → 367
992.85(10)[b]	0.671(25)	1007 → 14
994.7(3)[b]	0.19(3)	7646 → 6652
998.0(6)[c]	0.019(13)	5689 → 4692
1007.09(10)[b]	0.117(12)	4379 → 3371
1014.11(19)	0.099(13)	unplaced
1016.2(3)	0.12(3)	unplaced
1018.983(19)[b]	18.28(25)	1725 → 706
1021.93(18)[b]	0.077(12)	7646 → 6624
1028.5(3)[c]	0.43(13)	6075 → 5046
1030.73(20)	0.084(14)	unplaced
1032.66(21)[b]	0.073(14)	3240 → 2207
1056.9(3)[c]	0.027(13)	6365 → 5308

TABLE II. (*Continued.*)

E_γ (keV)	I_γ[a]	Placement (initial → final)
1062.05(24)[d]	0.056(13)	1198 → 136
1069.98(13)[c]	0.089(13)	2697 → 1627
1094.53(6)[c]	0.328(18)	3792 → 2697
1099.6(5)[c]	0.230(18)	6408 → 5308
1102.24(23)[c]	0.092(15)	5084 → 3982
1110.95(3)[b]	7.7(3)	2836 → 1725
1130.49(6)[b]	0.216(16)	7646 → 6516
1162.36(22)[c]	0.061(11)	4460 → 3298
1164.4(5)[b]	0.171(15)	3371 → 2207
1165(1)[b]	0.06(3)	7646 → 6481
1193.6(3)[c]	0.068(20)	5886 → 4692
1196.87(4)[c]	2.15(4)	2554 → 1357
1200.04(4)[d]	0.789(24)	2207 → 1007
1208.70(12)[b]	0.169(16)	2836 → 1627
1217.61(5)[c]	0.557(21)	3792 → 2574
1221.54(15)[b]	0.141(16)	3428 → 2207
1237.55(6)[b]	0.87(6)	7646 → 6408
1238.73(15)[c]	0.31(6)	4209 → 2971
1250.68(3)[b]	1.14(3)	1265 → 14
1253.9(3)[c]	0.067(16)	6746 → 5492
1256.83(20)[c]	0.104(17)	5238 → 3982
1260.535(21)[b]	25.2(3)	1627 → 367
1264.96(5)[b]	0.403(18)	1265 → 0
1268.38(19)[c]	0.090(18)	6314 → 5046
1277.15(11)[c]	0.125(15)	4460 → 3183
1281.31(4)[b]	0.851(23)	7646 → 6365
1284.0(5)[d]	0.5(2)	3982 → 2697
1288.61(20)[c]	0.065(13)	4209 → 2921
1293.32(4)[b]	0.299(25)	2921 → 1627
	1.09(3)	7646 → 6353
1300.06(17)[b]	0.110(14)	7646 → 6346
1309.77(17)[b]	0.078(14)	3428 → 2118
1324.96(24)[c]	0.078(15)	6408 → 5084
1328.0(3)[c]	0.048(14)	4249 → 2921
1332.34(8)[b]	0.317(17)	7646 → 6314
1342.78(7)[d]	0.682(22)	1357 → 14
1346.58(10)[c]	0.206(17)	7321 → 5975
1358.679(22)[b]	7.91(12)	1725 → 367
1361.6(3)[b]	0.079(20)	7646 → 6285
1364.69(6)[c]	0.344(19)	4548 → 3183
1373.5(3)[c]	0.050(17)	4209 → 2836
1380.46(18)[c]	0.116(19)	5629 → 4249
1407.72(5)[c]	0.345(14)	4379 → 2971
1411.85(4)[d]	2.02(3)	2118 → 706
1430.74(11)[b]	0.407(19)	7646 → 6215
1433.9(5)[c]	0.103(15)	5894 → 4460
1450.75(19)	0.092(15)	unplaced
1457.79(12)[b]	0.343(24)	3183 → 1725
1463.14(19)[c]	0.087(17)	5924 → 4460
1486.75(11)[b]	0.59(3)	7646 → 6160
1490.75(13)[b]	1.21(3)	1627 → 136
1511.49(2)	0.07(3)	unplaced
1513.9(5)[b]	0.34(3)	3240 → 1725
1529.15(11)[c]	0.167(16)	6837 → 5308
	0.167(16)	7646 → 6117

TABLE II. (*Continued.*)

E_γ (keV)	I_γ [a]	Placement (initial → final)
1542.18(19)[b]	0.088(16)	3660 → 2118
1549.36(19)[c]	0.100(16)	5689 → 4140
1555.70(8)[b]	0.185(17)	3183 → 1627
1571.02(4)[b]	0.513(23)	7646 → 6075
	0.13(3)	2836 → 1265
1574.34(21)	0.103(16)	unplaced
1582.82(22)[c]	0.104(23)	6408 → 4826
1584.60(3)[b]	0.21(3)	3792 → 2207
	0.85(3)	7646 → 6061
1589.05(3)[b]	0.668(19)	1725 → 136
1599.09(16)[c]	0.105(14)	6837 → 5238
1605.8(3)[c]	0.102(14)	7646 → 6040
1608.81(17)[b]	0.136(17)	7646 → 6037
	0.042(17)	5429 → 3820
1612.918(18)[b]	54.21(13)	1627 → 14
	0.41(9)	2971 → 1357
	1.25(13)	3240 → 1627
1616.82(16)[b]	0.114(16)	7646 → 6029
1624.28(21)[c]	0.111(20)	4460 → 2836
1627.34(4)[b]	3.33(6)	1627 → 0
1633.4(3)[b]	0.104(25)	7646 → 6013
1635.26(5)[c]	0.98(3)	4209 → 2574
1646.2(5)[b]	0.384(17)	3371 → 1725
1655.44(4)[d]	0.402(16)	2921 → 1265
	1.06(3)	4209 → 2554
1662.6(3)[c]	0.047(14)	4845 → 3183
1671.49(6)[b]	0.361(16)	7646 → 5975
1681.96(15)[d]	0.104(14)	4379 → 2697
1692.89(9)	0.148(17)	unplaced
1702.35(7)[b]	0.390(18)	3428 → 1725
1704.8(5)[d]	0.197(17)	4209 → 2505
1711.09(3)[b]	1.16(3)	1725 → 14
1721.1(3)[c]	0.27(10)	4692 → 2971
1722.65(4)[b]	3.89(9)	7646 → 5924
1725.459(18)[b]	64.1(9)	1725 → 0
1736.68(23)	0.095(16)	unplaced
1743.85(6)[b]	0.368(18)	3371 → 1627
1752.64(8)[b]	0.228(16)	7646 → 5894
1760.06(3)[b]	0.885(23)	7646 → 5886
1798.85(12)[b]	0.164(16)	2505 → 706
1824.26(14)[c]	0.154(16)	4379 → 2554
1840.62(5)[d]	0.592(22)	2207 → 367
1847.70(14)[c]	0.147(16)	2554 → 706
1851.78(4)[c]	0.580(21)	4773 → 2921
1856.04(4)[b]	0.671(23)	7646 → 5790
1863.18(21)[c]	0.088(16)	3982 → 2118
1867.76(25)[c]	0.069(15)	2574 → 706
1874.28(23)[c]	0.065(14)	4845 → 2971
1886.15(6)[c]	0.318(20)	4460 → 2574
1894.2(3)	0.056(19)	unplaced
1900.4(3)[c]	0.058(18)	6746 → 4845
1906.05(5)[c]	0.434(23)	4460 → 2554
1932.92(16)[b]	0.125(20)	7646 → 5713
1944.02(21)[c]	0.118(18)	5492 → 3547
1951.83(20)[b]	0.122(17)	4159 → 2207

TABLE II. (*Continued.*)

E_γ (keV)	I_γ [a]	Placement (initial → final)
1956.81(14)[b]	0.54(3)	7646 → 5689
1974.88(3)[b]	0.97(3)	3240 → 1265
1981.78(13)[c]	0.137(15)	2118 → 136
1991(1)[b]	0.16(6)	2697 → 706
2002.21(5)[b]	2.00(4)	4209 → 2207
2016.94(6)[b]	0.568(22)	7646 → 5629
2066.29(4)[b]	4.65(8)	3792 → 1725
2070.77(6)[c]	0.69(3)	2207 → 136
2075.64(12)[c]	0.171(24)	4773 → 2697
2091.18(5)[b]	2.05(4)	4209 → 2118
2103.83(6)[d]	0.79(3)	2118 → 14
2106.06(19)[b]	0.182(20)	3371 → 1265
2124.4(3)[b]	0.086(18)	7646 → 5522
2129.464(23)[b]	7.42(11)	2836 → 706
2138.19(3)[b]	2.40(5)	2505 → 367
2151.61(3)[b]	2.06(4)	7646 → 5495
2154.59(10)[b]	0.353(22)	7646 → 5492
2157.81(14)[c]	0.175(19)	7646 → 5488
2165(1)[b]	0.030(15)	7646 → 5482
2171.10(6)[b]	0.383(21)	4379 → 2207
2187.17(7)[c]	0.622(20)	4692 → 2505
2192.78(7)[d]	1.73(3)	2207 → 14
2197.7(4)[c]	0.036(15)	6746 → 4548
2207.36(10)[b]	0.48(3)	2207 → 0
	0.30(3)	2574 → 367
2209.90(16)[c]	0.03(3)	5046 → 2836
2217.26(11)[b]	0.278(22)	7646 → 5429
2254.60(17)[c]	0.174(22)	5495 → 3240
2260.18(8)[b]	0.415(25)	4379 → 2118
2264.28(5)[b]	0.67(3)	2971 → 706
2308.4(5)[c]	0.079(23)	5492 → 3183
2330.23(4)[b]	0.72(3)	2697 → 367
2338.04(6)[b]	0.315(20)	7646 → 5308
2354.6(3)[b]	0.055(18)	3982 → 1627
2361.77(20)	0.139(18)	unplaced
2368.42(4)[b]	0.726(25)	2505 → 136
2385.824(25)[b]	1.32(3)	7646 → 5260
2403.8(6)[c]	0.087(23)	6652 → 4249
2407.79(5)[b]	1.33(4)	7646 → 5238
2414.58(17)[b]	0.190(25)	4140 → 1725
2419.2(5)	0.035(22)	5790 → 3371
2424.16(5)[c]	1.01(3)	5260 → 2836
	0.51(3)	7646 → 5222
2433.72(14)[b]	0.26(3)	4159 → 1725
2437.53(13)[c]	0.25(3)	2574 → 136
2450.3(9)[c]	0.054(25)	5689 → 3240
2457.55(19)[b]	0.15(3)	4575 → 2118
2462.53(11)[c]	0.304(25)	3820 → 1357
2469.10(4)[b]	3.55(7)	2836 → 367
2472.3(3)[c]	0.11(3)	5308 → 2836
2477.7(10)[b]	0.14(3)	3183 → 706
2481(1)[b]	0.16(8)	7646 → 5164
2484.65(7)[b]	0.28(3)	4209 → 1725
	0.28(3)	4692 → 2207
2508.22(13)[c]	0.222(20)	5429 → 2921

TABLE II. (*Continued.*)

E_γ (keV)	I_γ[a]	Placement (initial → final)
2526.678(18)[b]	4.22(7)	3792 → 1265
2532(1)[b]	0.25(12)	4159 → 1627
2540.02(19)[c]	0.121(19)	3547 → 1007
2553.56(16)[b]	0.140(20)	2554 → 0
2562.53(11)[b]	0.41(4)	7646 → 5084
	0.16(4)	2697 → 136
2573.980(25)[d]	1.70(4)	2574 → 0
2582.06(4)[b]	0.85(3)	4209 → 1627
2600.00(14)[b]	0.189(20)	7646 → 5046
2603.88(4)[b]	0.78(3)	2971 → 367
2653.10(7)[b]	0.83(5)	4379 → 1725
2655.5(4)[b]	0.16(4)	4773 → 2118
2658.7(3)[c]	0.095(23)	5629 → 2971
2664.30(23)[b]	0.12(3)	3371 → 706
2682.599(18)[b]	4.30(7)	2697 → 14
	0.25(8)	7646 → 4964
2686.20(10)[c]	0.268(19)	5260 → 2574
2692.44(6)[d]	0.458(20)	6353 → 3660
2697.02(3)[b]	3.11(6)	2697 → 0
2699.50(10)[b]	0.55(4)	2836 → 136
2715.7(3)[b]	0.19(3)	4923 → 2207
2721.365(22)[b]	14.8(6)	3428 → 706
2724(1)[b]	0.34(11)	7646 → 4923
2734.72(4)[b]	1.59(7)	4460 → 1725
2751.05(4)[b]	1.43(6)	4379 → 1627
2766.44(19)[c]	0.18(3)	6314 → 3547
2800.62(6)[b]	0.81(4)	7646 → 4845
2813.77(7)[b]	1.06(5)	7646 → 4832
2816.1(5)[b]	0.12(5)	3183 → 367
2821.88(6)[b]	0.82(3)	7646 → 4826
2833.01(5)[b]	2.38(12)	4460 → 1627
2834.2(5)[b]	1.34(16)	2971 → 136
2835.9(5)[b]	5.42(10)	2836 → 0
2840.9(3)[b]	0.13(3)	3547 → 706
2849.9(3)[b]	0.14(3)	4575 → 1725
2873.49(4)[b]	3.79(7)	7646 → 4773
2894.12(11)[b]	0.296(22)	4159 → 1265
2905.96(18)[b]	0.217(23)	2921 → 14
2920.93(12)[b]	0.30(3)	2921 → 0
2944.48(8)[b]	0.78(3)	4209 → 1265
2953.97(7)[b]	0.19(9)	3660 → 706
	3.12(12)	7646 → 4692
2956.18(14)[b]	0.74(9)	2971 → 14
2966.83(21)[b]	0.37(4)	4692 → 1725
2970.29(7)[b]	1.54(7)	2971 → 0
3003.7(4)[b]	0.08(3)	3371 → 367
3047.4(3)[b]	0.11(3)	3183 → 136
3050.6(4)[c]	0.07(3)	4249 → 1198
3061.06(3)[b]	1.65(4)	3428 → 367
3070.85(6)[b]	0.89(3)	7646 → 4576
3074.6(6)[c]	0.063(23)	5629 → 2554
3095.2(3)	0.129(24)	unplaced
3098.38(16)[b]	0.34(3)	7646 → 4548
3103.38(4)[b]	6.63(12)	3240 → 136
3113.36(7)[b]	0.81(4)	4379 → 1265

TABLE II. (*Continued.*)

E_γ (keV)	I_γ[a]	Placement (initial → final)
3146.3(4)	0.047(22)	unplaced
3164.02(14)	0.29(3)	unplaced
3168.58(5)[b]	4.09(8)	3183 → 14
3172(1)[b]	0.22(11)	7646 → 4474
3182.7(3)[c]	0.29(9)	3183 → 0
3185.95(4)[b]	7.25(14)	7646 → 4460
3225.41(6)[b]	3.60(7)	3240 → 14
3234.4(3)[b]	0.184(25)	3371 → 136
3239.82(4)[b]	3.25(7)	3240 → 0
3267.43(4)[b]	13.33(22)	7646 → 4379
3275.4(5)	0.06(3)	unplaced
3283.71(11)[b]	0.46(3)	3298 → 14
3291.26(4)[b]	3.28(7)	3428 → 136
3298.16(11)[b]	0.45(3)	3298 → 0
3356.65(3)[b]	3.40(6)	3371 → 14
3371.21(7)[b]	0.23(3)	3371 → 0
	0.35(3)	4379 → 1007
3397.78(25)[b]	0.154(23)	7646 → 4249
3411(1)[b]	0.053(12)	3547 → 136
3413.321(25)[b]	16.9(3)	3428 → 14
3425(1)[b]	0.19(9)	3792 → 367
3427.58(21)[b]	0.23(3)	3428 → 0
3436.77(3)[b]	17.4(3)	7646 → 4209
3444.32(20)[c]	0.21(3)	6365 → 2921
3452.84(8)[b]	0.60(3)	3820 → 367
3486.92(5)[b]	4.24(9)	7646 → 4159
3502.70(5)[b]	1.95(5)	4209 → 706
3507.45(5)[b]	1.74(6)	4773 → 1265
	0.25(6)	7646 → 4140
3513.0(3)[b]	0.13(3)	5238 → 1725
3523.7(4)[c]	0.10(3)	3660 → 136
3533.2(3)[b]	0.11(3)	3547 → 14
3581.4(3)[b]	0.18(4)	3948 → 367
3612.0(5)[c]	0.11(3)	6117 → 2505
3615.03(13)[b]	0.40(3)	3982 → 367
3633.11(11)[b]	0.39(3)	5260 → 1627
3645.8(7)[c]	0.072(24)	3660 → 14
3654.2(3)[c]	0.043(24)	6160 → 2505
3664.38(5)[b]	1.32(4)	7646 → 3982
3671.9(3)[b]	0.137(25)	4379 → 706
3684.0(5)[b]	0.049(25)	3820 → 136
3697.57(17)[b]	0.28(3)	7646 → 3948
3710.9(3)[c]	0.35(4)	6408 → 2697
3753.57(19)[b]	0.214(25)	4460 → 706
3766.5(6)[c]	0.18(3)	5492 → 1725
3772.4(3)[b]	0.150(24)	4140 → 367
3777.26(4)[b]	2.83(6)	3792 → 14
3792.32(4)[b]	2.18(5)	4159 → 367
	0.03(1)	3792 → 0
3805.0(3)[b]	0.116(24)	5924 → 2118
3826.04(6)[b]	0.78(3)	7646 → 3820
3842.48(4)[b]	3.04(6)	4209 → 367
3845(1)[b]	0.06(3)	3982 → 136
3854.36(3)[b]	13.22(21)	7646 → 3792
3934.4(4)[b]	0.10(3)	3948 → 14

TABLE II. (*Continued.*)

E_γ (keV)	I_γ [a]	Placement (initial → final)
3956.77(12)[b]	0.52(3)	5222 → 1265
3962.6(5)	0.11(3)	unplaced
3967.3(3)[b]	0.25(3)	3982 → 14
3981.50(14)[b]	0.49(4)	3982 → 0
3985.3(4)[b]	0.31(3)	7646 → 3660
3995.3(4)[b]	0.12(3)	5260 → 1265
4011.9(3)[b]	4.19(8)	4379 → 367
4072.69(9)[b]	1.96(5)	4209 → 136
4093.47(19)[b]	0.31(3)	4460 → 367
4098.68(16)[b]	0.34(3)	7646 → 3547
4107(1)[b]	0.22(11)	4474 → 367
4111.8(6)[b]	0.09(3)	4249 → 136
4125.34(20)[b]	0.24(3)	4832 → 706
4145(1)[b]	0.09(3)	4159 → 14
4159.02(11)[b]	0.86(4)	4159 → 0
4194.71(7)[b]	0.85(4)	4209 → 14
4209.44(18)[b]	0.34(4)	4209 → 0
4218.19(4)[b]	36.9(6)	7646 → 3428
4242(1)[b]	0.10(3)	4379 → 136
4259.3(5)[b]	0.082(24)	5886 → 1627
4274.84(4)[b]	4.77(9)	7646 → 3371
4300.61(4)[c]	0.35(4)	5308 → 1007
4324.69(9)[b]	0.40(3)	4460 → 136
	0.21(3)	4692 → 367
4347.55(10)[b]	0.58(3)	7646 → 3298
4364.4(3)[b]	1.00(4)	4379 → 14
4378.69(6)[b]	2.35(6)	4379 → 0
4406.09(4)[b]	0.44(15)	4773 → 367
	16.3(3)	7646 → 3240
4411.1(8)[c]	0.12(4)	4548 → 136
4445.48(20)[b]	0.38(4)	4460 → 14
4458.79(20)[b]	1.06(10)	4824 → 367
4462.60(6)[b]	4.33(20)	7646 → 3183
	1.0(3)	4460 → 0
4531.9(3)[b]	0.44(3)	5238 → 706
4548(1)[b]	0.19(9)	4548 → 0
4555.6(3)[b]	0.99(5)	4692 → 136
4560.2(4)[b]	0.25(3)	4575 → 14
4575(1)[b]	0.13(3)	4575 → 0
4588.1(5)[c]	0.09(3)	6215 → 1627
4597(1)[b]	0.25(12)	4963 → 367
4639.41(25)[b]	0.25(3)	6365 → 1725
4658.52(9)[b]	0.83(4)	5924 → 1265
4675.29(6)[b]	4.22(8)	7646 → 2971
4679(1)[b]	0.10(5)	5046 → 367
4694.8(4)[b]	0.15(3)	4832 → 136
4725.69(24)[b]	0.17(3)	6353 → 1627
4772.49(12)[b]	0.60(4)	4773 → 0
4802.5(6)[c]	0.11(3)	6160 → 1357
4809.94(5)[b]	16.1(3)	7646 → 2836
4832.05(17)[b]	0.33(3)	4832 → 0
4845.21(14)[b]	0.41(3)	4845 → 0
4909(1)[b]	0.28(9)	4923 → 14
4923.1(6)[c]	0.13(3)	4923 → 0
4940.8(3)[b]	0.23(4)	5308 → 367
4948.81(9)[b]	7.32(13)	7646 → 2697
5069.2(3)[b]	0.26(5)	5084 → 14
5083(1)[b]	0.13(3)	5084 → 0
5100.6(4)[b]	0.13(4)	5238 → 136
5125(1)[b]	0.12(3)	5492 → 367
5127.2(6)[b]	0.14(5)	5495 → 367
5140.9(3)[b]	1.61(6)	7646 → 2505
5164(1)[b]	0.16(8)	5165 → 0
5179.46(21)[b]	0.34(4)	5886 → 706
5216.88(15)[b]	0.35(3)	5924 → 706
5223.66(21)[b]	0.27(3)	5238 → 14
5357.72(19)[b]	1.20(5)	5495 → 136
5429.1(4)[b]	0.19(4)	5429 → 0
5482(1)[b]	0.31(15)	5482 → 0
5488(1)[b]	0.17(3)	5488 → 0
5493.0(5)[b]	0.08(3)	5495 → 0
	0.18(4)	5629 → 136
5507.1(3)[b]	0.09(3)	5522 → 14
5525.2(9)[c]	0.07(5)	6790 → 1265
5553(1)[b]	0.07(2)	5689 → 136
5615(1)[b]	0.03(1)	5629 → 14
5646(1)[b]	0.09(3)	6013 → 367
5653.4(3)[b]	0.41(6)	5789 → 136
5673.3(5)[c]	0.38(6)	6040 → 367
5698.8(12)[b]	0.07(6)	5713 → 14
5749.5(3)[b]	0.19(4)	5886 → 136
5776(1)[b]	0.4(2)	5789 → 14
5786.76(10)[b]	0.88(5)	5924 → 136
5838.2(4)[b]	0.18(5)	5975 → 136
5886(1)[b]	0.24(8)	5886 → 0
5893(1)[b]	0.05(2)	5894 → 0
5909.7(8)[b]	0.22(6)	5924 → 14
5920.20(5)[b]	80.7(16)	7646 → 1725
5922.7(3)[b]	1.3(5)	5924 → 0
5998.0(7)[b]	0.14(5)	6013 → 14
6018.43(5)[b]	82.4(13)	7646 → 1627
6029(1)[b]	0.12(3)	6029 → 0
6037(1)[b]	0.16(8)	6038 → 0
6046.9(3)[b]	0.24(4)	6062 → 14
6061.07(15)[b]	0.61(5)	6062 → 0
6073.8(7)[b]	0.12(4)	6075 → 0
6103(1)[b]	0.12(6)	6117 → 14
6117(1)[b]	0.21(3)	6117 → 0
6144.7(3)[b]	0.28(5)	6160 → 14
6200.5(4)[b]	0.31(6)	6215 → 14
6285(1)[b]	0.08(3)	6285 → 0
6314(1)[b]	0.17(3)	6314 → 0
6338.05(23)[b]	0.60(3)	6353 → 14
6345(1)[b]	0.06(3)	6482 → 136
6346(1)[b]	0.08(3)	6346 → 0
6365(1)[b]	0.16(8)	6365 → 0
6380.63(8)[b]	7.18(13)	7646 → 1265
6393.7(5)[b]	0.12(4)	6408 → 14
6407.4(5)[b]	0.20(4)	6408 → 0
6501.1(6)[b]	0.18(5)	6516 → 14

TABLE II. (*Continued.*)

E_γ (keV)	I_γ [a]	Placement (initial → final)
6610(1) [b]	0.08(3)	6624 → 14
6652(1) [b]	0.13(3)	6652 → 0
6661(1) [b]	0.14(3)	6676 → 14
6701.4(5)	0.12(4)	6837 → 136
6710(1) [b]	0.12(6)	6725 → 14
6731(1) [b]	0.24(4)	6746 → 14
6753.5(5) [b]	0.06(2)	7120 → 367
6764(1) [b]	0.09(3)	6778 → 14
6837(1) [b]	0.06(3)	6837 → 0
6939(1) [b]	0.47(15)	7646 → 706
7278.76(19) [b]	48(3)	7646 → 367
7306.5(6) [b]	0.32(7)	7321 → 14
7312.7(9) [c]	0.22(8)	7313 → 0
7554.2(5) [c]	0.13(5)	7555 → 0
7631.06(8) [b]	228(4)	7646 → 14
7645.48(8) [b]	200(3)	7646 → 0

[a]Relative intensity. For multiply placed transitions the singles γ-ray intensity has been divided on the basis of intensity balance and coincidence data. Multiply by 0.1190(7) for transition probability per 100 neutron captures, $P_\gamma(\%)$.
[b]Transition confirmed by coincidence data.
[c]Transition placed by energy sums.
[d]Transition adopted from ENSDF [12].

2920.60-keV levels were not seen in either the singles or coincidence measurements. The method of placement of each γ ray in the decay scheme is noted in Tables I and II.

Data for 97 levels and the neutron capture state in ^{57}Fe are summarized in Table III. Level energies were determined by a least-squares fit of the recoil-corrected γ-ray energies to the level scheme. The spins and parities of the ^{57}Fe levels in Table III are discussed in the ENSDF evaluation [12] and are based on all experimental reaction and decay data populating ^{57}Fe, including the results discussed here. The intensity balance reported in Table III has been corrected for internal conversion including internal pair conversion (IPC) [13] which varies 0.13–0.26% for $E1$ and $M1$ transitions with energies of 3.0–7.6 MeV.

We found that ≈33 levels assigned to ^{57}Fe by Vennink *et al.* [6] could not be confirmed by this work, while an approximately equal number of new levels were added to the ^{57}Fe level scheme. Many of the new levels involved different placements of γ rays first observed by Vennink *et al.*, demonstrating the fallibility of relying on energy sums for γ-ray placement and the necessity of coincidence data for reliable construction of a level scheme.

A. Intensity balance

The γ-ray transition intensities have been corrected for a small contribution from internal conversion, calculated with the BRICC code [13], assuming either experimentally determined multipolarities or $M1$, $E1$, or $E2$ depending on the initial and final level spins and parities. When the spin or parity of the initial or final levels was unknown, $E1$ multipolarity

TABLE III. Level energies, J^π, and intensity balance per 100 neutron captures feeding/deexciting levels in ^{57}Fe.

E_{level} (keV)	J^π	P_γ(in)	P_γ(out)	P_γ(in-out)
0.0	$1/2^-$	101.0(10) [a]		
14.399(7)	$3/2^-$	62.4(9) [a]	62.4(9) [a]	0.0(17)
136.444(10)	$5/2^-$	4.67(4)	4.93(7)	− 0.26(8)
366.747(9)	$3/2^-$	15.2(4)	15.26(17)	0.0(4)
706.418(12)	$5/2^-$	6.89(8)	7.07(8)	− 0.19(12)
1007.22(5)	$7/2^-$	0.227(14)	0.230(6)	− 0.003(17)
1198.39(24)	$9/2^-$	0.008(4)	0.0067(15)	0.002(4)
1265.009(15)	$1/2^-$	2.256(23)	2.49(4)	− 0.24(4)
1357.20(9)	$7/2^-$	0.386(13)	0.388(13)	− 0.002(19)
1627.292(16)	$3/2^-$	10.79(16)	10.91(4)	− 0.11(16)
1725.449(15)	$3/2^-$	10.95(19)	11.05(11)	− 0.09(22)
2118.27(3)	$5/2^-$	0.383(0)	0.391(6)	0.008(11)
2207.24(4)	$5/2^-$	0.438(9)	0.510(7)	− 0.071(11)
2504.95(3)	$5/2^+$	0.381(9)	0.399(7)	− 0.018(12)
2554.12(25)	$3/2^-$	0.209(6)	0.290(6)	− 0.081(8)
2574.069(24)	$(3/2)^-$	0.277(6)	0.276(7)	0.001(9)
2697.069(17)	$1/2^-$	1.05(3)	1.017(14)	0.04(3)
2835.935(22)	$3/2^{(+)}$	2.09(4)	2.264(21)	− 0.18(4)
2920.56(7)	$1/2^-,3/2^-$	0.150(6)	0.145(6)	0.005(8)
2970.60(7)	$3/2^-$	0.653(17)	0.65(3)	0.00(3)
3183.07(4)	$1/2^-,3/2^-$	0.587(24)	0.628(17)	− 0.04(3)
3239.911(21)	$1/2^-$	1.97(4)	2.030(25)	− 0.06(4)
3298.28(8)	$(1/2^+,3/2^+)$	0.087(4)	0.108(5)	− 0.021(7)
3371.17(4)	$3/2^-$	0.597(11)	0.610(11)	− 0.013(16)
3427.840(17)	$3/2^-$	4.42(7)	4.47(8)	− 0.05(11)
3547.43(9)	$3/2^-$	0.076(6)	0.076(7)	0.000(9)
3660.23(25)	$(5/2^+)$	0.091(4)	0.054(12)	0.038(13)
3791.747(19)	$3/2^+$	1.576(25)	1.584(19)	− 0.007(18)
3819.59(25)	$(5/2^+)$	0.098(4)	0.114(6)	− 0.16(7)
3948.49(16)	$(5/2^+)$	0.033(4)	0.033(6)	0.000(7)
3981.66(5)	$3/2^-$	0.184(6)	0.219(25)	− 0.04(3)
4140.01(15)	$5/2^+$	0.042(7)	0.041(4)	0.002(8)
4159.20(3)	1/2,3/2	0.505(11)	0.486(17)	0.019(20)
4209.355(25)	$3/2^-$	2.07(4)	2.003(18)	0.07(4)
4248.78(7)	$5/2^{(+)}$	0.044(5)	0.039(6)	0.005(8)
4378.54(4)	$3/2^-$	1.59(3)	1.514(18)	0.07(3)
4460.24(3)	$(1/2^-,3/2^-)$	0.887(17)	0.87(4)	0.02(4)
4474.0(10)	$(5/2^+)$	0.026(13)	0.026(13)	0.000(18)
4547.79(7)	$1/2^-$,3/2	0.064(6)	0.081(12)	− 0.017(13)
4575.87(17)	$1/2^-$,3/2	0.106(4)	0.080(7)	0.026(8)
4692.13(5)	$(3/2)^+$	0.382(15)	0.327(16)	0.055(22)
4772.62(4)	$(3/2^+)$	0.451(8)	0.440(21)	0.011(22)
4825.5(3)	$1/2^+,3/2^+$	0.12(4)	0.126(12)	− 0.01(4)
4832.30(8)	$3/2^-$	0.126(6)	0.086(6)	0.040(9)
4845.47(6)	1/2,3/2	0.103(5)	0.062(4)	0.041(7)
4922.9(3)	$1/2^-$,3/2	0.040(13)	0.071(12)	− 0.031(18)
4963.6(3)	$(5/2^+)$	0.030(10)	0.030(14)	0.000(17)
5046.00(12)	(1/2)	0.084(16)	0.015(7)	0.069(17)
5083.63(10)	$1/2^+$,3/2	0.058(5)	0.059(7)	− 0.001(8)
5164.0(10)	$1/2^+$	0.019(10)	0.019(10)	0.000(14)
5221.75(25)	1/2,3/2	0.061(4)	0.062(4)	− 0.001(6)
5238.34(6)	$1/2^-$,3/2	0.171(5)	0.147(9)	0.024(11)
5260.31(3)	1/2,3/2	0.157(4)	0.213(7)	− 0.056(7)
5308.08(6)	$(3/2^-)$	0.090(4)	0.082(8)	0.008(9)
5428.82(10)	$3/2^+$	0.054(3)	0.054(6)	0.000(7)
5482.0(7)	1/2,3/2	0.0036(18)	0.037(18)	− 0.033(18)

TABLE III. (*Continued.*)

E_{level} (keV)	J^π	P_γ(in)	P_γ(out)	P_γ(in-out)
5488.37(25)	1/2,3/2	0.0208(23)	0.020(4)	0.001(4)
5491.55(10)	1/2,3/2	0.050(3)	0.059(6)	− 0.009(7)
5494.53(4)	$1/2^-$,3/2	0.245(5)	0.192(10)	0.053(11)
5521.8(3)	$1/2^+$	0.0102(21)	0.011(4)	− 0.001(4)
5629.23(7)	3/2	0.068(3)	0.058(7)	0.010(7)
5689.40(14)	3/2	0.064(4)	0.029(5)	0.035(6)
5713.23(18)	$(1/2^+)$	0.0149(24)	0.008(7)	0.007(8)
5790.1(3)	1/2,3/2	0.080(3)	0.101(25)	0.021(25)
5886.10(4)	$1/2^-$,3/2	0.105(3)	0.109(12)	− 0.004(12)
5893.53(9)	1/2,3/2	0.0271(19)	0.018(3)	0.009(4)
5923.51(4)	$1/2^-$,3/2	0.463(11)	0.45(6)	0.01(6)
5974.67(7)	$(3/2^+)$	0.067(3)	0.021(6)	0.046(7)
6012.8(3)	1/2,3/2	0.012(3)	0.027(7)	− 0.015(8)
6029.36(25)	$3/2^+$	0.0136(19)	0.014(4)	0.000(4)
6037.4(3)	1/2,3/2	0.0162(20)	0.019(10)	− 0.003(10)
6040.3(3)	1/2,3/2	0.0245(21)	0.045(7)	− 0.021(7)
6061.47(15)	1/2,3/2	0.101(4)	0.101(8)	0.000(9)
6074.7(3)	1/2,3/2	0.061(3)	0.065(16)	− 0.004(16)
6117.02(12)	$1/2^+$,3/2	0.0199(19)	0.052(9)	− 0.032(9)
6159.55(13)	$3/2^-$	0.070(4)	0.073(8)	− 0.003(9)
6215.42(12)	$1/2^+$	0.0484(23)	0.048(8)	0.000(8)
6284.6(6)	1/2,3/2	0.0094(24)	0.0010(4)	− 0.0006(24)
6313.86(9)	1/2,3/2	0.0377(20)	0.052(6)	− 0.015(6)
6346.11(19)	1/2,3/2	0.0131(17)	0.010(4)	− 0.004(4)
6352.85(5)	1/2,3/2	0.130(4)	0.146(6)	− 0.016(7)
6364.87(5)	$3/2^+$	0.101(3)	0.077(11)	0.024(11)
6408.36(17)	$3/2^+$	0.104(7)	0.129(9)	− 0.025(12)
6481.0(10)	1/2,3/2	0.007(4)	0.007(4)	0.000(6)[c]
6515.68(7)	$3/2^+$	0.0257(19)	0.021(6)	− 0.004(6)
6624.2(3)	1/2,3/2	0.0092(14)	0.010(4)	− 0.001(4)
6651.7(3)	$1/2^+$,3/2	0.023(4)	0.026(5)	− 0.003(6)
6675.70(25)	$3/2^+$	0.0171(23)	0.017(4)	0.000(4)
6724.0(10)	1/2,3/2	0.014(7)	0.014(7)	0.000(1)[c]
6745.50(7)	1/2,3/2	0.0386(24)	0.048(6)	− 0.009(6)
6778.4(3)	1/2,3/2	0.0102(23)	0.011(4)	− 0.001(4)
6790.29(19)	1/2,3/2	0.0113(18)	0.008(6)	− 0.003(6)
6837.34(11)	$1/2^-$,3/2	0.055(18)	0.054(7)	0.000(19)[c]
7120.3(3)	1/2,3/2	0.0075(14)	0.0071(24)	0.000(3)
7313.2(8)	1/2,3/2	0.026(10)[c]	0.026(10)	0.000(14)[c]
7321.27(13)	1/2,3/2	0.063(24)[c]	0.063(24)	0.00(3)[c]
7554.4(3)	1/2,3/2	0.015(6)[c]	0.015(6)	0.000(9)[c]
7646.183(18)[b]	$1/2^+$		99.5(8)	

[a]Corrected for unobserved statistical feeding as described in the text.
[b]Neutron capture energy.
[c]Primary γ-ray populating level was not observed. The intensity is from the intensity balance.

was assumed. The total observed primary transition intensity depopulating the capture state is $98.5 \pm 1.3\%$ of that seen feeding the ground and 14-keV states, indicating that the level scheme is nearly complete. The intensity of the 23 unplaced transitions is only 0.14% of the total placed transition intensity.

To estimate the unobserved transition intensity contribution to the ^{57}Fe decay scheme, we have plotted the intensity per 100 neutron captures, $P_\gamma(\%)$, from the renormalized intensities in Tables I and II (see footnote "a"), for all γ rays, primary γ rays, and γ rays feeding the GS and 14-keV levels in order of decreasing $P_\gamma(\%)$ value in Fig. 1. Each of these $P_\gamma(\%)$ distributions can be fit to a simple exponential. The fitting parameters for these four exponential fits are summarized in Table IV. In each fit we have ignored both the most intense γ rays, which deviate from an exponential fit, and the least intense ≈10% transitions, above a cutoff N_{cut}. The weakest transitions may not all be observed, which is consistent with Fig. 1 where, above N_{cut}, the $P_\gamma(\%)$ values begin to fall below the exponential trend. Integrating the exponential fits from N_{cut} to a maximum number of transitions, N_{max} gives an estimate of the total missing transition probability. For the primary, GS, and 14-keV level transitions we assume $N_{max} = 330$,

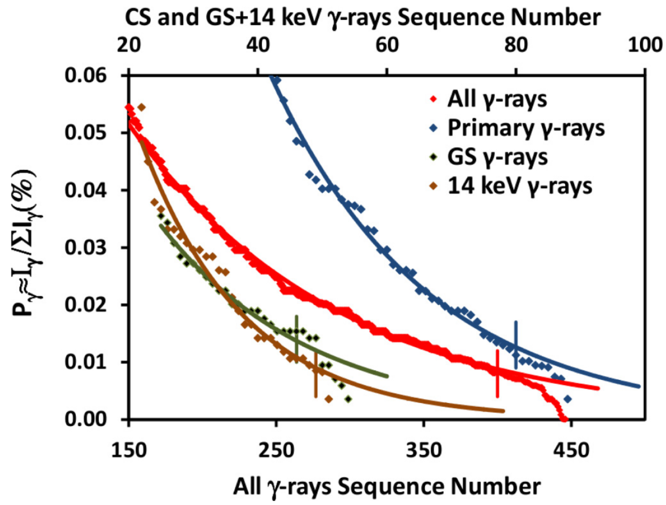

FIG. 1. Plot of ^{57}Fe transition probabilities, $P_\gamma(\%)$, ordered by their decreasing value, for all, primary, ground state (GS), and 14-keV level feeding γ rays. The solid lines through each plot represent an exponential fit through the data below N_{cut}, indicated by the vertical lines in each curve. Extrapolation of the fit to higher γ-ray numbers gives an estimate of the unobserved feeding. The parameters of each exponential fit are given in Table IV.

TABLE IV. The $P_\gamma(\%)$ distribution for all, primary (CS), ground state (GS), and 14-keV level feeding γ rays have been fit to an exponential defined as $P_\gamma(\%) = ae^{-bN}$ where N is the γ-ray number in decreasing intensity. N_γ is the total number of transitions observed in each category. The unobserved contribution was calculated by integrating the exponential from a cutoff transition number, N_{cut}, to a maximum number of transitions, N_{max}, and subtracting the intensity of transitions experimentally observed above N_{cut}.

	Parameters a	b	N_γ	N_{cut}	$\sum_{N_{cut}}^{N_\gamma} P_\gamma(\%)$ expt	calc	$\sum_{N_{cut}}^{N_{max}} P_\gamma(\%)$ netcalc[a]	netcalc-expt[b]
All	0.015	0.071	448	397	0.28	0.37	1.27	0.99
CS	0.35	0.041	89	80	0.08	0.11	0.32	0.25
GS	0.12	0.049	55	42	0.08	0.11	0.32	0.18
14	0.098	0.042	51	46	0.040	0.058	0.33	0.29

[a]$N_{max} = 330$ for GS, 14 keV, and CS transitions, and 1000 for all transitions.
[b]Total unobserved percent transition probability.

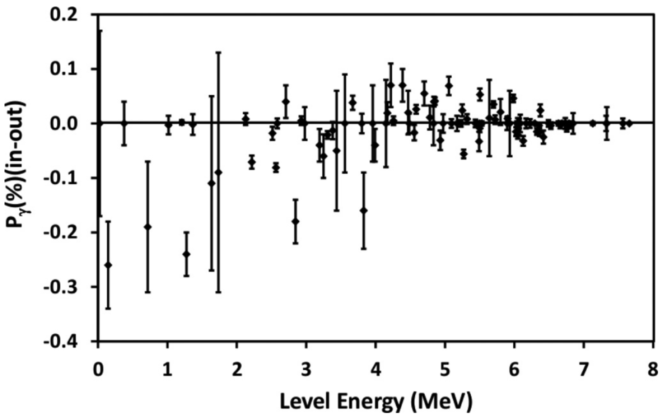

FIG. 2. The $P_\gamma(\%)$ balance populating/depopulating levels in ^{57}Fe following thermal neutron capture.

the number of levels that can be fed by a dipole transition according to the constant temperature (CT) model prediction, and we arbitrarily limit the total number of transitions to $N_{\max} = 1000$. The integral is not very sensitive to the choice of $N_{\max}$ because the transition probability is observed to fall off very rapidly with transition number. The theoretical justification for this estimate is discussed below.

The calculated missing transition probabilities are summarized in Table IV. For the total observed γ-ray spectrum we estimate that $\approx$1% of the total transition probability is missing. This is remarkably consistent with the total observed γ-ray energy production, $\Sigma P_\gamma(\%)E_\gamma/(100 \times S_n) = 0.989 \pm 0.014$, where S_n is the neutron separation energy. We calculate the total missing primary γ-ray transition probability $\Delta P_\gamma(\%)(\mathrm{CS}) = 0.25\%$. For γ rays feeding the GS + 14 keV levels the missing transition probability is $\Delta P_\gamma(\%)(\mathrm{GS} + 14) = 0.47\%$. This missing transition probability is consistent with the variations in the transition probability balance shown in Fig. 2 and lower than the statistical uncertainty in the total primary and GS + 14 keV level feedings. For the ^{56}Fe(n,γ) decay scheme the average γ-ray multiplicity per neutron capture is $M_\gamma = \sum P_\gamma(\%)/100 = 1.83$ and the total multiplicity, including internal conversion, is $M_{\gamma+e} = \sum P_{\gamma+e}(\%)/100 = 2.39$.

The γ-ray intensities in Tables I and II are normalized relative to 100 for the 352.347-keV γ-ray and can be renormalized to percent transition probabilities, $P_\gamma(\%)$, by the factor 0.1190 ± 0.0007, assuming that the sum of the observed GS + 14 keV level feedings and CS deexcitation transition probabilities, $P_\gamma(\mathrm{GS} + 14 + \mathrm{CS})\% = 200$, after correcting for the missing transition probabilities as described above. The transition probability balance through all proposed levels in ^{57}Fe is shown in Table III and summarized in Fig. 2. The decay scheme is very well balanced, with discrepancies of $\Delta P_\gamma(\%) \lesssim 0.3\%$ through all levels.

B. ^{56}Fe(n,γ) cross section

Two independent internal calibrations of the ^{56}Fe$(n,\gamma)^{57}$Fe γ-ray cross sections were performed with iron(III) acetylacetonate ($C_{15}H_{21}FeO_6$) and iron pyrite (FeS_2) targets. The iron(III) acetylacetonate target, provided by Sigma-Aldrich, was certified as 99.9% pure on a trace metals basis, but the purity of the Fe(III) oxidation state was not explicitly given. Iron(III) acetylacetonate is 15.812(2)% Fe by weight; however, the certified Fe content was 16.0(2)%, which is consistent with the target containing $<6.1\%$ iron(II) acetylacetonate ($C_{10}H_{14}FeO_4$). This suggests a target H/Fe ratio of 20.78 ± 0.22. Using the 2223.2-keV γ ray from the ^{1}H(n,γ) reaction, assuming $\sigma_\gamma(2223) = 0.3325(7)$ b [14], we determined the 352.3-keV γ-ray cross section to be 0.2844(19) b.

Iron pyrite occurs only in the Fe(II) oxidation state since the Fe(III) sulfide is unstable and does not appear in nature. From our prompt γ-ray measurements on the pyrite target we set a limit of $<0.5\%$ for sulfide impurities. Using the 841-keV γ ray from the ^{32}S(n,γ) reaction, assuming $\sigma_\gamma(841) = 0.353(2)$ b [15], we determined $\sigma_\gamma(352) = 0.2858(26)$ b. The weighted average of these two measurements is $\sigma_\gamma(352) = 0.2849(15)$ b. This value together with $P_\gamma(352) = 11.90 \pm 0.07\%$ from the level scheme normalization gives the ^{56}Fe(n,γ) total radiative cross section as $\sigma_0 = 2.394(19)$ b. This measured cross section is independent of the neutron flux for a homogenous target since it is only dependent on the ratio of ^{1}H and ^{32}S standardization cross sections to the 352-keV γ-ray transition probability. The guided neutron beam energy used in these measurements is subthermal energy so no correction was necessary for epithermal contributions to the measured γ-ray cross sections.

Only three measurements of ^{56}Fe(n,γ) were found in the literature, 2.65(8) b by Pomerance [16] based on the pile oscillator method, which has been renormalized to the modern ^{197}Au(n,γ) cross section calibration standard [17], 2.57(14) b by Shcherbokov *et al.* [18], based on a time-of-flight measurement, and 2.51(4) b [15] by Revay and Molnár based on an earlier prompt γ-ray measurement. The recommended cross section from Mughabghab [17] is 2.59(14) b. All previous values are significantly higher than our measurement, which has a considerably smaller uncertainty.

C. ^{57}Fe neutron separation energy

A weighted least-squares fit of the recoil-corrected γ-ray energies to obtain the level energies in ^{57}Fe determined the neutron separation energy for the capture state to be 7646.183(18) keV. This value is slightly higher than the adopted value of 7646.08(4) keV from the 2013 mass evaluation by Wang *et al.* [19].

IV. STATISTICAL MODEL TESTS

The transition probabilities observed in this work can be compared with calculated values using the Monte Carlo computer code DICEBOX [20]. DICEBOX is based on the generalization of the extreme statistical model embodying Bohr's idea of a compound nucleus [21]. We have simulated the decay of the ^{57}Fe capture state with several photon strength function models. Here we show results only for simulations with a combination of the Kadmenskij-Markushev-Furman (KMF) $E1$ photon strength function (PSF) [22] and the

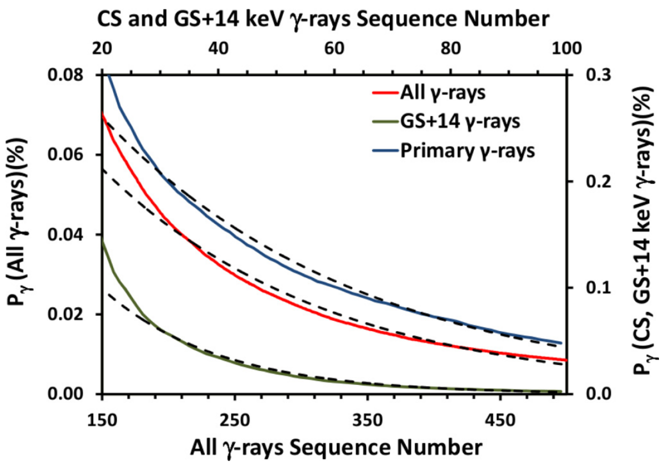

FIG. 3. Plot of simulated ^{57}Fe transition probabilities, $P_\gamma(\%)$, ordered by decreasing value for all, primary, and GS + 14 keV level feeding γ rays and averaged over 40 realizations with model A. The dashed black lines through each plot are an exponential fit through the predictions.

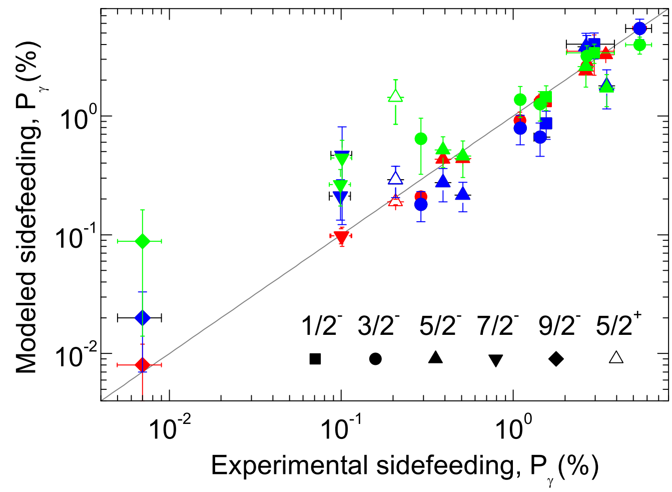

FIG. 4. Simulated vs experimental side-feeding transition probabilities, $P_\gamma(\%)$. The modeled side-feeding corresponds to the predicted feeding from levels above $E_{\rm crit}$ except for the capture state. Experimental side-feeding corresponds to the difference between the intensity deexciting levels below $E_{\rm crit}$, minus the capture state feeding, and the feeding intensity from levels below $E_{\rm crit}$. Calculations were done using models A (blue markers) and B (green markers) that are described in the text. The observed side-feeding is shown (red markers) for comparison.

single-particle (SP) model [23] $M1$ PSF, labeled model A, and a PSF model based on the Oslo data [24] with an "upbend" of $M1$ origin, labeled model B. Levels in both models were generated using the constant temperature (CT) level density (LD) model [25]. The spins and parities of levels below an excitation energy $E_{\rm crit} = 2.56$ MeV, where the level scheme is believed to be complete, are from the recent ^{57}Fe ENSDF evaluation [12], while the γ-ray transition probabilities deexciting levels below $E_{\rm crit}$ and primary transition probabilities feeding these levels are taken from this work. Above $E_{\rm crit}$, individual levels were generated using the LD model, and transition probabilities were obtained using Monte Carlo method assuming the Porter-Thomas (PT) distribution [26] around expectation values given by the PSF model. Random fluctuations can produce an infinite number of different artificial sets of levels and decay intensities called nuclear realizations. Typically 40 different nuclear realizations were simulated for each combination of PSFs and LD models. The number of cascades in each realization was 10^6.

In Fig. 3 we have plotted ordered transition probabilities, averaged over 40 nuclear realizations, for all γ rays, primary γ rays, and γ rays feeding the GS + 14 keV levels, as predicted by model A. Each set of transitions can reasonably be fit with an exponential, as we observed in Fig. 1 and discussed in Sec. III A. Predictions for individual nuclear realizations significantly vary in magnitude, some agreeing with experiment. However, the shapes of predictions are similar for all nuclear realizations. Predictions with model B show a similar exponential trend although the absolute magnitude does not agree as well with experiment. These calculations reinforce the validity of our method for estimating the missing transition intensity.

Simulations can also be used to investigate the intensity balance through levels below $E_{\rm crit}$. We can compare the simulated feeding of these levels from levels above $E_{\rm crit}$, excluding the capture state that is taken from experiment, with the missing experimental feeding from levels below $E_{\rm crit}$. The missing experimental feeding is defined as the difference between the intensity deexciting a level and the intensity populating that level from levels below $E_{\rm crit}$ and from the capture state. We call these quantities the modeled and experimental side-feedings, which should ideally be equal. The side-feeding comparison, expressed as $P_\gamma(\%)$, for both A and B models is shown in Fig. 4. Modest agreement between the experimental and modeled side-feedings indicates that the statistical model calculations using available models of the PSF and level density are adequate in ^{57}Fe. There is a general trend for levels with higher experimental side-feeding to have higher simulated side-feedings, indicating that the statistical model can reasonably predict the population of low-lying levels even for light nuclei like ^{57}Fe. A better description of experimental data is obtained with model B except for the side-feeding of the $5/2^+$ state. The $5/2^+$ state is the lowest excited positive parity state, suggesting that discrepancies may arise from the LD model, which does not consider the parity distribution. Similar side-feeding agreement was also obtained with the other tested PSF models. The observed side-feeding, defined as above but using the experimental population from levels above $E_{\rm crit}$ instead of the simulated feedings, is also shown in Fig. 4. This side-feeding is well balanced, showing that the experimental side-feeding is well determined and simulated side-feeding discrepancies are largely due to inadequacies in the models.

There are more variables that could be used for testing various PSF and LD models within statistical model calculations and possibly the validity of the statistical model itself. However, such an analysis goes beyond the scope of this paper and will be published separately.

V. CONCLUSIONS

The ^{56}Fe(n,γ) reaction has been investigated using cold neutron beams and γ-ray singles and coincidence measurements. A detailed ^{57}Fe capture state decay scheme has been constructed where ≈99% of the γ-ray transition intensity has been placed. Approximately 33 previously adopted levels in ^{57}Fe could not be confirmed in this work while a comparable number of new levels were added. This improvement is largely the result of our coincidence data which was not available in earlier work. Internal standardization of the measured intensities in the singles spectrum with γ-ray cross section standards has determined the ^{57}Fe total radiative thermal neutron capture cross section as $\sigma_0 = 2.394 \pm 0.019$ b. This cross section includes a small correction for unobserved continuum transitions. The experimental population of low-lying levels, below $E_{\text{crit}} = 2.56$ MeV, has been compared to statistical model calculations with modest agreement.

ACKNOWLEDGMENTS

This work was performed under the auspices of the US Department of Energy by the University of California, supported by the Director, Office of Science, Office of Basic Energy Sciences, of the US Department of Energy at Lawrence Berkeley National Laboratory under Contract No. DE-AC02-05CH11231. Support was also provided by Grant No. 13-07117S of the Czech Science Foundation and by NAP-VENEUS Contract No. OMFB-00184/2006 of Hungary. The $\gamma\gamma$ coincidence experiment was carried out at the CANAM infrastructure of the NPI ASCR Řež, supported by the Ministry of Education, Youth and Sports (Project No. LM2011019). The enriched ^{56}Fe target was provided by Dr. Frank Gunsing, CERN, and obtained on loan from the Instituto de Fisica Corpuscular, University of Valencia, courtesy of J. L. Tain.

[1] T. Belgya, Z. Révay, I. H. B. Fazekas, L. Dabolczi, G. Molnár, J. O. Z. Kis, and G. Kaszás, in *Proceedings of the 9th International Symposium on Capture Gamma-Ray Spectroscopy and Related Topics*, Budapest, Hungary, October 8–12, 1996, edited by G. Molnár, T. Belgya, and Zs. Révay (Springer-Verlag, Berlin, 1997), p. 826.

[2] Z. Révay, T. Belgya, Z. Kasztovszky, J. Weil, and G. Molnár, Nucl. Instrum. Methods Phys. Res., Sect. B **213**, 385 (2004).

[3] R. B. Firestone, H. D. Choi, R. M. Lindstrom, G. L. Molnár, S. F. Mughabghab, R. Paviotti-Corcuera, Z. Révay, V. Zerkin, and C. M. Zhou, *Database of Prompt Gamma Rays from Slow Neutron Capture for Elemental Analysis*, STI/PUB/1263 (IAEA, Vienna, 2007).

[4] *Handbook of Prompt Gamma Activations Analysis with Neutron Beams*, edited by G. Molnár (Kluwer Academic, Boston, 2004).

[5] M. Kostal, J. Milcak, V. Rypar, V. Juricek, M. Svadlenkova, A. Kolros, and B. Jansky, Nucl. Data Sheets **118**, 561 (2014).

[6] R. Vennink, J. Kopecky, P. Endt, and P. Glaudemans, Nucl. Phys. A **344**, 421 (1980).

[7] F. Bečvář, J. Honzátko, M. Krtička, S. Pasic, G. Rusev, and I. Tomandl, Nucl. Instrum. Methods Phys. Res., Sect. B **261**, 930 (2007).

[8] G. Molnár, Z. Révay, and T. Belgya, Nucl. Instrum. Methods Phys. Res., Sect. A **489**, 140 (2002).

[9] B. Fazekas, J. Óstór, Z. Kis, G. Molnár, and A. Simonits, in *Proceedings of the 9th International Symposium on Capture Gamma-Ray Spectroscopy and Related Topics*, Budapest, Hungary, October 8–12, 1996, edited by G. Molnár, T. Belgya, and Zs. Révay (Springer-Verlag, Berlin, 1997), p. 774.

[10] K. Rosman and P. Taylor, Pure Appl. Chem. **70**, 217 (1998).

[11] J. Honzátko, K. Konečný, I. Tomandl, J. Vacík, F. Bečvář, and P. Cejnar, Nucl. Instrum. Methods Phys. Res., Sect. A **376**, 434 (1996).

[12] A. Negret, R. Firestone, and B. Singh, Nucl. Data Sheets (to be published).

[13] T. Kibédi, T. Burrows, M. Trzhaskovskaya, P. Davidson, and J. C. W. Nestor, Nucl. Instrum. Methods Phys. Res., Sect. A **589**, 202 (2008).

[14] R. B. Firestone and Z. Revay, Phys. Rev. C **93**, 044311 (2016).

[15] Z. Révay and G. Molnár, Radiochim. Acta **91**, 361 (2003).

[16] H. Pomerance, Phys. Rev. **88**, 412 (1952).

[17] S. Mughabghab, *Atlas of Neutron Resonances*, 5th ed. (Elsevier, New York, 2006).

[18] O. Shcherbakov, A. Stupak, and A. Glukhovec, Jadernye Konstanty **25**, 51 (1977).

[19] M. Wang, G. Audi, A. Wapstra, F. Kondev, F. MacCormick, X. Xu, and B. Pfeiffer, Chin. Phys. C **36**, 1603 (2012).

[20] F. Bečvář, Nucl. Instrum. Methods Phys. Res., Sect. A **417**, 434 (1998).

[21] N. Bohr, Nature (London) **137**, 344 (1936).

[22] S. Kadmenskij, V. P. Markushev, and V. I. Furman, Sov. J. Nucl. Phys. **37**, 165 (1983).

[23] J. Blatt and V. Weisskopf, *Theoretical Nuclear Physics* (John Wiley and Sons, New York, 1952).

[24] M. Guttormsen, A. Larsen, J. Rekstad, S. Siem, N. Syed, A. Schiller, and A. Voinov, PoS PSF07, 003 (2007).

[25] A. Gilbert and A. Cameron, Can. J. Phys. **43**, 1446 (1965).

[26] C. Porter and R. Thomas, Phys. Rev. **104**, 483 (1956).